

Identifying recombination parameters by injection-dependent lifetime spectroscopy on mc-silicon based on photoluminescence imaging

Marie Syre Wiig, Halvard Haug, Rune Søndena, and Erik S. Marstein

Citation: *AIP Conference Proceedings* **1999**, 130017 (2018); doi: 10.1063/1.5049336

View online: <https://doi.org/10.1063/1.5049336>

View Table of Contents: <http://aip.scitation.org/toc/apc/1999/1>

Published by the *American Institute of Physics*

Articles you may be interested in

[Lifetime degradation in multicrystalline silicon under illumination at elevated temperature: Indications for the involvement of hydrogen](#)

AIP Conference Proceedings **1999**, 130001 (2018); 10.1063/1.5049320

[Improving transient photoconductance lifetime measurements on ingots with deeper photogeneration](#)

AIP Conference Proceedings **1999**, 020008 (2018); 10.1063/1.5049247

[Temperature coefficients in compensated silicon solar cells investigated by temperature dependent lifetime measurements and numerical device simulation](#)

AIP Conference Proceedings **1999**, 020010 (2018); 10.1063/1.5049249

[Gettering of interstitial iron in silicon by plasma-enhanced chemical vapour deposited silicon nitride films](#)

Journal of Applied Physics **120**, 193103 (2016); 10.1063/1.4967914

[A generalized model for boron-oxygen related light-induced degradation in crystalline silicon](#)

AIP Conference Proceedings **1999**, 130006 (2018); 10.1063/1.5049325

[Modeling of light-induced degradation due to Cu precipitation in p-type silicon. II. Comparison of simulations and experiments](#)

Journal of Applied Physics **121**, 195704 (2017); 10.1063/1.4983455

AIP | Conference Proceedings

Get **30% off** all
print proceedings!

Enter Promotion Code **PDF30** at checkout



Identifying Recombination Parameters by Injection-Dependent Lifetime Spectroscopy on Mc-Silicon Based on Photoluminescence Imaging

Marie Syre Wiig,^{1, a)} Halvard Haug¹, Rune Søndena¹ and Erik S. Marstein^{1, 2}

¹*Institute for Energy Technology, Instituttveien 18, 2007 Kjeller, Norway*

²*Institute for Technology Systems, University of Oslo, 2007 Kjeller*

^{a)}Corresponding author: marie.syre.wiig@ife.no

Abstract. The minority carrier lifetime is a crucial material parameter in silicon (Si) wafers for use in solar cell applications, and precise measurements of carrier lifetime as a function of the excess carrier concentration (injection level) is of high importance. In this paper we present a method for extracting injection-dependent lifetime data with high spatial resolution, without the need for advanced time-resolved camera detection systems. This enables investigations of single grains, grain boundaries and structural defects in wafers with spatially non-uniform lifetime, such as high performance multicrystalline Si wafers. The local injection dependent lifetime curves are constructed from a series of photoluminescence images acquired using different steady state generation rates, carefully calibrated by a secondary quasi-steady state photoconductance measurement at a fixed light intensity. The local lifetime has been analyzed by linear parameterization of the Shockley-Read-Hall recombination model and solved for all combinations of defect parameters describing the observed recombination behavior. The recombination parameters found to dominate at high injection corresponds well with published recombination parameters due to Cr.

INTRODUCTION

Injection-level dependent measurements of the effective carrier lifetime are necessary in order to predict and analyse solar cell performance at the excess carrier concentration obtained under the conditions in which the solar cell operates. Furthermore, injection-dependent lifetime spectroscopy (IDLS) is a powerful technique for investigation of Shockley Read Hall (SRH) defect recombination parameters, and can in many cases be used for identification of detrimental impurities¹⁻⁶. The rate of SRH recombination depends on the product of the defect concentration (N_t) and the capture cross sections for each carrier type ($\sigma_{n,p}$). Lifetime spectroscopy methods show a high sensitivity to all electrically active defects, even if their concentration lies below the detection limit of direct concentration measurements, such as deep level transient spectroscopy (DLTS)³.

In recent years, there has been a shift towards growth of multi-crystalline silicon (mc-Si), so-called high performance multi-crystalline silicon (HPMC-Si), in the photovoltaic industry. HPMC-Si offers increased control of the grain size and grain orientation reducing dislocation growth, thus reducing overall recombination losses and ultimately increasing the performance of the final cells^{7,8}. As a result of modified casting processes, grain sizes are smaller in HPMC-Si relative to conventional mc-Si^{9,10}. In conventional mc-Si, the overall lifetime has long been known to increase after phosphorus diffusion gettering (PDG) due to removal of metallic impurities¹¹⁻¹³. However, in HPMC-Si the average lifetime has been shown to decrease in the middle section of the block after PDG^{14,15}. This is a combined effect of lower initial impurity concentration in current industrial casts, and the increased density of grain boundaries (GBs) in HPMC Si material.

The quasi-steady state photoconductance (QSSPC) method is a well-established technique for performing IDLS measurements^{16,17}. However the applicability to non-uniform mc-Si and HPMC Si is limited by the diameter of the

QSSPC coil. With a standard QSSPC measurement it is not possible to perform quantitative and spatially resolved analysis of the effect of PDG on bulk grains and on GBs.

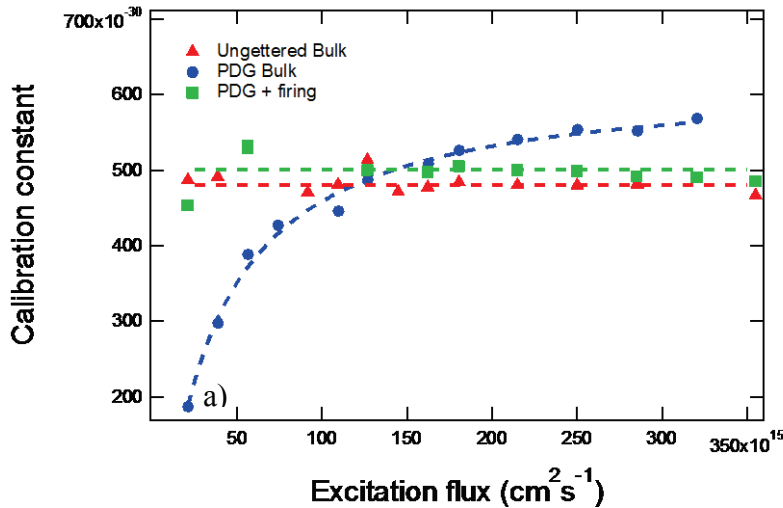
Photoluminescence (PL) imaging is a fast and powerful technique for studying the carrier lifetime in Si wafers and cells with high spatial resolution¹⁸. The small grain size in industrial HPMC-Si wafers requires high resolution analysis methods in order to understand local material properties. In this work we have combined PL-imaging with QSSPC measurements of the lifetime in order to extract IDLS data from an area of just a few μm . Moreover, the resulting lifetime maps were corrected for lateral diffusion of carriers toward highly recombination active GBs. This enables IDLS analysis of specific grains, GBs or crystal defects in mc-Si and HPMC Si. The lifetime data for selected regions of interest were analysed based on linear parameterization⁴ of the lifetime finding the defect parameter solution surfaces (DPSS) for two locally dominating defect centres.

EXPERIMENTAL DETAILS

In this work, we illustrate local analysis of recombination properties by performing spatially resolved lifetime spectroscopy on HPMC-Si wafers cut from approximately 50% of the height of an ingot. Neighbouring wafers were processed to three different stages of the solar cell process. One was left ungettered, another subjected to PDG and a third subjected to both PDG and a subsequent hydrogen passivation of the GBs (PDG and fired). The hydrogen passivation was achieved in a simulated contact firing process with a peak temperature close to 800 °C with a hydrogen rich SiN_x anti reflection coating (ARC)/passivation layer present. Before lifetime measurements, the ARC were removed and the emitter etched back before the surfaces were passivated with 40 nm a-Si:H layers on both sides, processed by plasma enhanced chemical vapour deposition (PECVD). To make sure that the chemical state of any defects was stable during imaging, the samples were illuminated to stabilize light-induced degradation (LID) and to split all FeB pairs before PL-images were acquired. PL images were acquired with a LIS-R1 from BT imaging using a high magnification lens imaging a $2 \times 2 \text{ cm}^2$ area with a resolution of $20 \mu\text{m}/\text{pixel}$. A 1050 nm short pass filter was in place during the measurements. For the local analysis, the PL signal was averaged over a radius of $200 \mu\text{m}$ (10 pixels).

The PL signal emitted (I_{PL}) is directly related to the excess carrier density (Δn) by¹⁹;

$$I_{PL,rel} = \frac{Bt(N_A + \Delta n)\Delta n}{A_i} = Ct(N_A + \Delta n)\Delta n \quad (1)$$



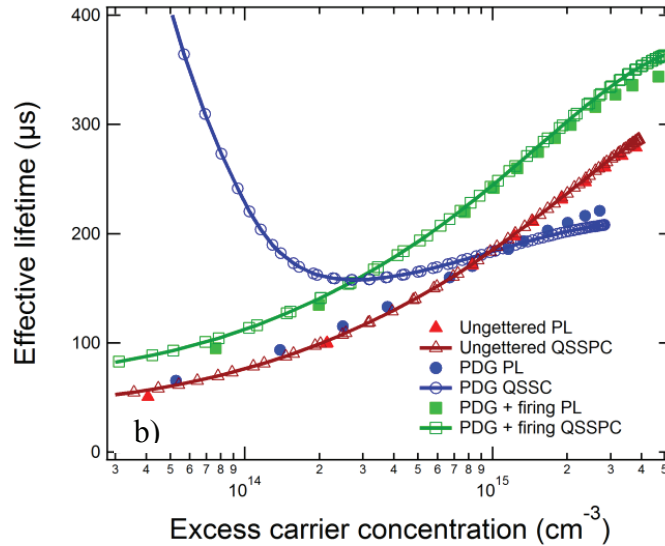


FIGURE 1. a) Calibration constant as a function of generation rate. Ungettered (red triangles, after PDG (blue dots) and after PDG and fired (green squares). The lines are a guide to the eye. b) Effective lifetime vs. excess carrier concentration after three different stages of solar cell processing. The filled symbols are from PL-images, whereas open symbols + lines are from QSSPC measurements.

Where N_A is the doping concentration and Δn is the excess carrier concentration. The calibration factor A_i is system specific. Since the radiative recombination coefficient (B) is also constant for moderate injection levels¹⁹, B/A_i can be grouped as one calibration constant (C) which applies to all samples with the same thickness and optical properties independent of excess carrier concentration. t is the integration time for the PL signal over which the image is acquired²⁰.

Fig. 1a shows the calculated calibration constant at increasing photon flux, based on the value of I_{PL} from the areas of the HPMC-Si wafer that covers the inductive coil. The calibration constant calculated for the ungettered and the PDG and fired samples is as expected independent of the injection level. The mean calibration constant for these two samples deviates by 4%, which is acceptable. However, the calibration constant shows strong injection dependence in the case of the PDG wafer. All three samples are from neighboring positions in a block with equal doping and optical properties after etching. One reason for the strong injection dependence at low injection observed for the PDG sample is the artificially high lifetime measured in the reference QSSPC measurement caused by trapping, as described above²¹⁻²³. Such trapping effects are negligible in PL-signals for the typical resistivity and defect density in mc-Si material for solar cells, thus causing a mismatch in low injection between the two measured values²³. Another reason for the injection dependence of the calibration constant for the PDG sample is the observed activation of strong recombination at and in the vicinity of GB's, which results in large lifetime variations above the calibration coil. This causes a non-linear contribution from laterally varying Δn to the voltage induced in the coil, an effect which influences the measurements at all injection levels.

For each pixel, or set of pixels over which signals are averaged, it is then possible to construct the injection level dependent lifetime curve without influence of trapping. As shown in Fig. 1b this method gives a good correspondence with the QSSPC measurements for the two samples which are not influenced by trapping, thus providing a verification of the method.

As the PL signal is not affected by trapping in the same manner as QSSPC, data unaffected by trapping can be extracted also for samples otherwise dominated by trapping artefacts at low injection, which typically is seen for samples with large in-homogeneities and highly recombination active grain boundaries. Fig. 1 shows injection dependent lifetime measured by QSSPC, compared with data from a series of PL-images averaged over signal the signal from the area covered by the coil. For the sample subjected to PDG, the QSSPC measurement was affected by trapping. However, after the above-mentioned correction, the data from the PL-images show no such effects and can be used for further analysis of the recombination centers.

An obvious advantage of this method is that extraction of the injection dependent lifetime is not restricted to the region above the coil. After correct calibration the local injection dependence can be evaluated separately, thus enabling injection dependent lifetime measurements with high spatial resolution. Calibration of the PL signal to the

carrier lifetime may also be done in a purely optical manner using a finely time-resolved detection system²⁴, and similar measurements has previously been published utilizing time-resolved camera detection systems^{25,26}. However most experimental setups operate in steady state and QSSPC calibration of steady state images greatly simplifies the measurement system¹⁶.

DATA ANALYSIS

Local analysis of a small grain was performed on a wafer after PDG. The excess carrier profile was measured across a grain perpendicular to a highly recombination active GB. A PL-image of the sample and the position of the measured carrier profile is indicated in Fig 2a. Fig 2b shows the carrier profile perpendicular to a recombination active GB, together with the simulated diffusion profile and the corresponding fitted recombination profile. PL-images were acquired at different generation rates and the bulk lifetime in the grain was found from a fit between the diffusion equation, Eq (2), and the measured carrier profiles²⁷.

$$\frac{n}{\tau_R} = G + D\nabla^2 n \quad (2)$$

Where n is the carrier concentration, τ_R the recombination profile and G the generation rate.

From Fig 2b it can be seen that the peak lifetime from the PL-image underestimates the intra-grain lifetime in a small grain by approximately 10% in this specific case. As the generation rate increases, the diffusion of carriers toward the GB increases and the deviation between measured and actual lifetime increases. Fig. 2c shows the measured (blue circles) injection-dependent lifetime in a grain small grain together with the lifetime corrected for diffusion (red squares) of carriers perpendicular to a highly recombination active GB. For very small grains simultaneously affected by multiple GBs, this diffusion correction should be extended to a 2D simulation.

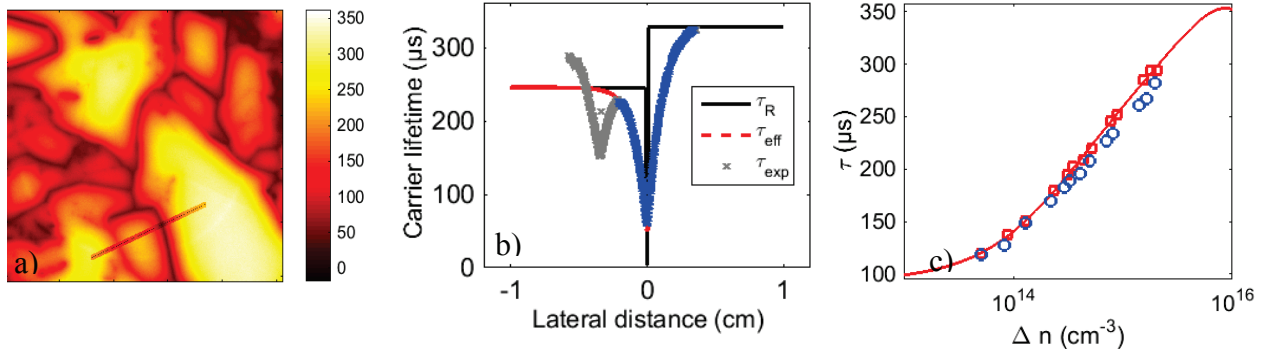


FIGURE 2. a) PL-image of 2x2 cm area, the line indicates where the carrier profile has been measured b) grey - measured steady state carrier profile, blue - carrier profile used for simulations of recombination profile and black - the fitted recombination profile. c) Injection dependent lifetime curve, blue circles – from raw data and red squares – simulated bulk lifetime. The solid red line corresponds to two defect fit of the lifetime according to the solution in Fig. 3.

After calculating the de-smearred bulk lifetime removing the contribution from carrier diffusion, the SRH recombination was calculated from the effective lifetime by correcting for intrinsic recombination, Eq. 3²⁸. From τ_{SRH} two dominating recombination centers were separated by linear parameterization of SRH recombination according to Murphy⁴ described by Eq 4:

$$\frac{1}{\tau_{eff}} - \frac{1}{\tau_{intr}} = \frac{1}{\tau_{SRH,1}} + \frac{1}{\tau_{SRH,2}} \quad (3)$$

$$\tau_{SRH}(X, T) = \tau_{0n} \left(1 + \frac{kn_1}{p_0} + \frac{p_1}{p_0} \right) + \tau_{0n} \left(k - \frac{kn_1}{p_0} - \frac{p_1}{p_0} \right) X \quad (4)$$

$$X = \frac{n}{p} = \frac{\Delta n}{p_0 + \Delta n} \quad k = \frac{v_{th,e} \left(\xi + \frac{p_1}{p_0} \right)}{v_{th,h} \left(1 - \frac{n_1}{p_0} - \xi \right)} \quad \xi = \frac{d\tau}{dX} \Big|_{\lim X \rightarrow 1} \quad (5-7)$$

where X is the ratio between electron and hole concentration and k is the ratio between the capture cross section for holes and electrons.

The lifetime due to each of the two defects is shown as the dotted blue and dashed green lines in Fig. 3a. The solid black line is the fitted effective lifetime i.e. the inverse sum of the two linear defects. The defect parameter solution surfaces³ (DPSS) were calculated from Eq. 5-7, where ζ is a defect parameter describing the injection dependence for the defect, independent of defect concentration. The DPSSs in Fig 3b, shows all combinations of k at energy level (E_t), which describes the two linear parameterizations (blue and green curves) in Fig 3a. The points indicated in Fig. 3b corresponds to recombination parameters for known defect centers reported in the literature; however for some of the recombination centers the reported literature values have a large scatter. The selected literature values are given in Table 1.

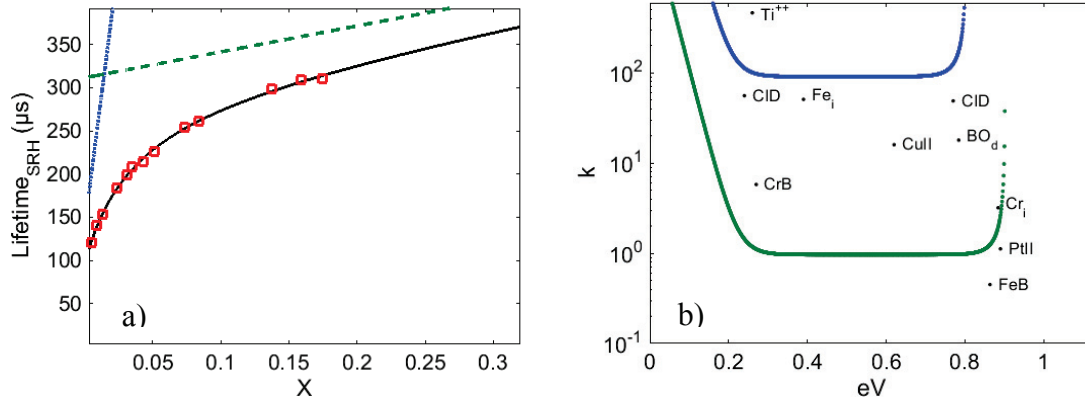


FIGURE 3. a) Linear parameterization of the lifetime before gettingting showing a two defect fit. b) DPSS for two dominating recombination centers corresponding to the parameterization in a).

TABLE 1. Literature values for SRH recombination parameters.

Defect	E _t -E _v	k	Ref	Defect	E _t -E _v	k	Ref
Fe _i	0.39	51	29	Ti ⁺⁺	0.26	464	30
CID	0.24	56	31	Cr _i	0.88	3.2	32
CID	0.77	49	31	CrB	0.27	5.8	32
BO _d	0.784	18	33	CuII	0.62	16	34
BO _a	0.24	0.017	33	PtII	0.89	1.12	35
FeB	0.8634	0.45	36				

The DPSSs describes two deep defects, where the defect dominating the lifetime at high injection can be well described by recombination due to interstitial Cr_i. The approach describes an accurate methodology for calibrating lifetime images and how to obtain local injection dependent lifetime data for identification of locally dominating recombination centers. By increasing the number of measurement points in high injection the robustness of the defect identification could have been improved further.

Due to diffusion of carriers from regions with high lifetime to low lifetime areas, the signal from highly recombination active grain boundaries in steady state PL-images underestimates the recombination activity. A realistic lifetime at the grain boundary was found by fitting the steady state minority carrier profile perpendicular to the GB with equations for transport of carriers³⁷.

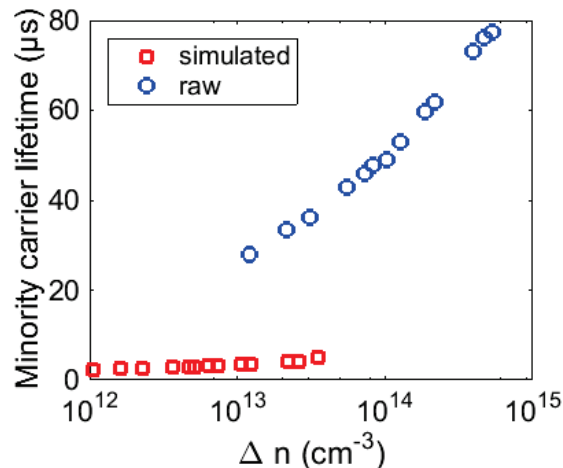


FIGURE 4. Lifetime measured at GB in steady state PL-image (blue circles) and – lifetime corrected for transport of carriers according to simulated recombination profile (red squares).

The measured and simulated lifetime at the GB is shown in Fig. 4, the simulated effective lifetime data show a limited injection range between 1×10^{12} and $5 \times 10^{13} \text{ cm}^{-3}$ as a result of the low effective lifetime. The magnitude of this simulated lifetime at the GB depends on the defined width of the recombination profile. From images of samples limited by surface recombination velocity with short diffusion length a width of $100 \mu\text{m}$ was found to be reasonable¹⁴.

Due to the limited injection range below 5×10^{13} it was not possible to identify the SRH recombination centers exactly at the strongly recombination active grain boundary.

CONCLUSION

A methodology combining local injection dependent lifetime imaging with linear parameterization of the SRH recombination parameters in order to better understand and quantify spatially varying recombination in inhomogeneous mc-Si material has been demonstrated. The method for spatially resolved DPSS shows a large potential. Potential SRH defects corresponding to the recombination in the material has been identified in the larger grains using DPSS. However, in order to improve the robustness of the method and the applicability to analysis of recombination at the different grain boundaries the injection range of the photoluminescence imaging has to be extended. The intra-grain lifetime was corrected to remove the influence of strong recombination in the surrounding grain boundaries, this is especially important for small grains.

REFERENCES

1. L. E. Mundt, M. C. Schubert, J. Schön, B. Michl, T. Niewelt, F. Schindler, and W. Warta, *IEEE Journal of Photovoltaics* **5**, 1503 (2015).
2. A. Inglese, J. Lindroos, H. Vahlman, and H. Savin, *Journal of Applied Physics* **120**, 125703 (2016).
3. S. Rein, *Lifetime spectroscopy: a method of defect characterization in silicon for photovoltaic applications*, Vol. 85 (Springer Science & Business Media, 2006).
4. J. D. Murphy, K. Bothe, R. Krain, V. V. Voronkov, and R. J. Falster, *Journal of Applied Physics* **111**, 113709 (2012).
5. J. Schön, A. Youssef, S. Park, L. E. Mundt, T. Niewelt, S. Mack, K. Nakajima, K. Morishita, R. Murai, M. A. Jensen, T. Buonassisi, and M. C. Schubert, *Journal of Applied Physics* **120**, 105703 (2016).
6. J. Schmidt, *Applied Physics Letters* **82**, 2178 (2003).
7. C. W. Lan, W. C. Lan, T. F. Lee, A. Yu, Y. M. Yang, W. C. Hsu, B. Hsu, and A. Yang, *Journal of Crystal Growth* **360**, 68 (2012).
8. G. Stokkan, Y. Hu, Ø. Mjøs, and M. Juel, *Solar Energy Materials and Solar Cells* **130**, 679 (2014).

9. Y. M. Yang, A. Yu, B. Hsu, W. C. Hsu, A. Yang, and C. W. Lan, [Progress in Photovoltaics: Research and Applications](#) **23**, 340 (2015).
10. Y. T. Wong, C. Hsu, and C. W. Lan, [Journal of Crystal Growth](#) **387**, 10 (2014).
11. A. Bentzen and A. Holt, [Materials Science and Engineering: B](#) **159–160**, 228 (2009).
12. M. Syre, S. Karazhanov, B. R. Olaisen, A. Holt, and B. G. Svensson, [Journal of Applied Physics](#) **110** (2011).
13. S. Gindner, P. Karzel, B. Herzog, and G. Hahn, [Photovoltaics, IEEE Journal of](#) **4**, 1063 (2014).
14. M. S. Wiig, K. Adamczyk, H. Haug, K. E. Ekstrøm, and R. Søndena, [Energy Procedia](#) **92**, 886 (2016).
15. R. Søndena, J. Gjessing, H. Angelskår, Ø. Norseth, S. E. Foss, and E. S. Marstein, in *28th European Photovoltaic Solar Energy Conference and Exhibition* (Paris, 2013).
16. R. A. Sinton, A. Cuevas, and M. Stuckings, in *Quasi-steady-state photoconductance, a new method for solar cell material and device characterization*, 1996, p. 457.
17. A. Cuevas and D. Macdonald, [Solar Energy](#) **76**, 255 (2004).
18. T. Trupke, R. A. Bardos, M. C. Schubert, and W. Warta, [Applied Physics Letters](#) **89**, 044107 (2006).
19. T. Trupke, R. A. Bardos, and M. D. Abbott, [Applied Physics Letters](#) **87**, 184102 (2005).
20. H. C. Sio, S. P. Phang, T. Trupke, and D. Macdonald, [Solar Energy Materials and Solar Cells](#) **131**, 77 (2014).
21. D. Macdonald and A. Cuevas, [Solar Energy Materials and Solar Cells](#) **65**, 509 (2001).
22. R. Gogolin, N. P. Harder, and R. Brendel, in *Trapping-related recombination of charge carriers in silicon*, 2010, p. 000443.
23. R. A. Bardos, T. Trupke, M. C. Schubert, and T. Roth, [Applied Physics Letters](#) **88** (2006).
24. J. A. Giesecke, B. Michl, F. Schindler, M. C. Schubert, and W. Warta, [Energy Procedia](#) **8**, 64 (2011).
25. S. Herlufsen, K. Bothe, R. Brendel, and J. Schmidt, [Energy Procedia](#) **55**, 77 (2014).
26. J. A. Giesecke, M. C. Schubert, B. Michl, F. Schindler, and W. Warta, [Solar Energy Materials and Solar Cells](#) **95**, 1011 (2011).
27. H. Angelskår, R. Søndena, M. S. Wiig, and E. S. Marstein, [Energy Procedia](#) **27**, 160 (2012).
28. A. Richter, F. Werner, A. Cuevas, J. Schmidt, and S. W. Glunz, [Energy Procedia](#) **27**, 88 (2012).
29. S. Rein and S. W. Glunz, [Journal of Applied Physics](#) **98**, 113711 (2005).
30. A. C. Wang and C. T. Sah, [Journal of Applied Physics](#) **56**, 1021 (1984).
31. C. Vargas, Y. Zhu, G. Coletti, C. Chan, D. Payne, M. Jensen, and Z. Hameiri, [Applied Physics Letters](#) **110**, 092106 (2017).
32. C. Sun, F. E. Rougieux, and D. Macdonald, [Journal of Applied Physics](#) **115**, 214907 (2014).
33. B. Hallam, M. Kim, M. Abbott, N. Nampalli, T. Nærland, B. Stefani, and S. Wenham, [Solar Energy Materials and Solar Cells](#) **173**, 25 (2017).
34. J. Schmidt, B. Lim, D. Walter, K. Bothe, S. Gatz, T. Dullweber, and P. P. Altermatt, in *Impurity-related limitations of next-generation industrial silicon solar cells*, 2012, p. 1.
35. K. Graff, *Metal Impurities in Silicon-Device Fabrication* (Springer, New York 1995).
36. S. Diez, S. Rein, T. Roth, and S. W. Glunz, [Journal of Applied Physics](#) **101** (2007).
37. M. S. Wiig, H. Haug, R. Søndena, and E. S. Marstein, [Energy Procedia](#) **124**, 215 (2017).